AIP | Review of Scientific Instruments

Heavy ion beam probe energy analyzer for measurements of plasma potential fluctuations

L. Solensten and K. A. Connor

Citation: Review of Scientific Instruments **58**, 516 (1987); doi: 10.1063/1.1139262
View online: http://dx.doi.org/10.1063/1.1139262
View Table of Contents: http://scitation.aip.org/content/aip/journal/rsi/58/4?ver=pdfcov
Published by the AIP Publishing

Heavy ion beam probe energy analyzer for measurements of plasma potential fluctuations

L. Solensten and K. A. Connor

Plasma Dynamics Laboratory, Rensselaer Polytechnic Institute, Troy, New York 12180

(Received 6 June 1986; accepted for publication 22 December 1986)

The operation of a Proca and Green type 30° parallel plate electrostatic energy analyzer is modeled in a new manner that permits high-resolution heavy ion beam probe measurements of fluctuating plasma potential. Systematic calibration procedures permit detection of potential changes smaller than 0.01% of the probing beam energy at frequencies up to a megahertz. Most recent applications of beam probes have made use of this new capability.

INTRODUCTION

Heavy ion beam probes have been used for some time to obtain spatially resolved measurements of plasma potential $\phi(\bar{r})$, electron density $n_e(\bar{r})$, and temperature $T_e(\bar{r})$.[1] Recently, measurements of the time dependence of ϕ and total detected signal, which is a function of electron density and temperature, have also been made.[2]

The basic configuration of a heavy ion beam probe is illustrated in Fig. 1. A primary beam of singly charged ions (R^+) is directed across the confining magnetic field into the plasma chamber. As the beam passes through the plasma, a fraction of the ions undergo ionizating collisions with plasma particles to produce ions of higher charge states (R^{n+1}) which are separated from the primary ions by the confining field.

A small aperture detector, located outside the magnetic field, collects particles of a particular charge originating in a small piece of the primary beam, thereby providing excellent spatial resolution. The amount of R^{n+1} ion flux (usually R^{+2}) collected is proportional to the effective cross section for the dominant ionization process (electron impact) and the density of the target particles. The energy of the secondary ions leaving the plasma exceeds that of the primary ions by an amount equal to $ne\phi(\bar{r})$, where $\phi(\bar{r})$ is the plasma potential at the point of ionization. Thus if the detector in a heavy ion beam probe system is an energy analyzer, it is possible to directly determine $\phi(\bar{r})$.

All recent applications of heavy ion beam probes have used a parallel plate electrostatic energy analyzer of the type shown in Fig. 2.[3] The broad, two-dimensional spray of ions created by collisions between the primary beam and plasma electrons is collimated into a narrow beam by the aperture in the lower left. The beam passes through a field-free drift region into a region of constant electric field which directs it back to detector plates located in the field-free region. The analyzer is operated in two modes. In the first, the voltage on the top plate V_A is adjusted until the currents on the two plates are equal ($i_L = i_U$). V_A and the geometry of the analyzer then determine the ion energy. In the second, V_A is set such that the beam falls at least partially on both plates. The two currents i_L and i_U are measured. V_A, i_L, i_U, and the analyzer geometry determine the ion energy. The second technique is significantly faster than the first because the two currents can be measured more rapidly than the voltage V_A can be changed.

I. ANALYZER MODEL

Ideal analyzer operation is based on solution of single ion trajectories that pass through some part of the entrance aperture and end somewhere on the detector plates. Position in the aperture is labeled l with $l = 0$ at the center and $l = \pm w/2$ at the edges of an aperture of width w. Position on the detector plates is labeled s with $s = 0$ at the gap between the two plates; $s < 0$ on the upper plate and $s > 0$ on the lower plate. The relationship between l and s for a general ion trajectory (energy $= E_I$) is

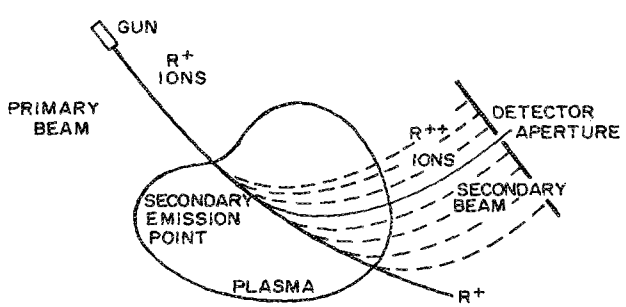

FIG. 1. Heavy ion beam probe geometry.

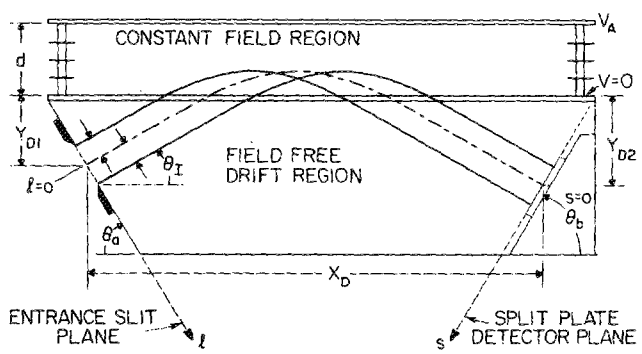

FIG. 2. Electrostatic energy analyzer geometry.

 0034-6748/87/040516-04$01.30

$$s=\frac{X_D \tan\theta_I(l)-l\left[\sin\theta_a+\cos\theta_a\tan\theta_I(l)\right]-Y_D-4E_I(l)d\sin^2\theta_I(l)/q_sV_A}{\sin\theta_b+\cos\theta_b\tan\theta_I(l)}. \tag{1}$$

$\theta_I(l)$ is the angle of the trajectory passing through l measured with respect to the ground plane. $X_D, Y_D = Y_{D1}+Y_{D2}$, θ_a, θ_b, and d are geometric constants. q_s is the charge of the ion.

Equation (1) can be used to find the dependence of ion energy on the two currents i_L and i_U. Those ion trajectories that intersect the lower plate pass through the aperture between $l=-w/2$ and $l(s=0)$ while those for the upper plate fall between $l=+w/2$ and $l(s=0)$ (see Fig. 3). Evaluating (1) for $s=0$, we obtain

$$l(s=0)=\frac{X_D\tan\theta_I-Y_D-4E_Id\sin^2\theta_I/q_sV_A}{\sin\theta_a+\cos\theta_b\tan\theta_I}. \tag{2}$$

As long as the plasma density and temperature do not change significantly over the small sample volume, the ion current density in the aperture will be uniform. In this case,

$$\frac{i_L}{i_L+i_U}=\frac{l(s=0)+w/2}{w},\quad \frac{i_U}{i_L+i_U}=\frac{w/2-l(s=0)}{w}. \tag{3}$$

It is now only necessary to combine Eqs. (2) and (3) to obtain the dependence of ion energy E_I on the two detected currents. However, it is more useful to determine the relationship between the plasma potential and these currents. For a heavy ion beam probe, the energy of the secondary ion entering the analyzer is[4]

$$E_I=q_pV_G+(q_s-q_p)\phi, \tag{4}$$

where V_G is the accelerator voltage, q_p the charge of the ion injected into the plasma, and q_s the ion charge after colliding with a plasma electron. Usually $q_s=2e$ and $q_p=e$. The expression for ϕ is then

$$\phi=\frac{-q_sV_A}{(q_s-q_p)}\times\left(\frac{i_L-i_U}{i_L+i_U}\frac{w(\sin\theta_a+\cos\theta_a\tan\theta_I)}{8d\sin^2\theta_I}+\frac{Y_D-X_D\tan\theta_I}{4d\sin^2\theta_I}\right)-\frac{q_pV_G}{q_s-q_p}. \tag{5}$$

This can be simplified to

$$\phi=\frac{+q_sV_A}{(q_s-q_p)}\left(\frac{-i_L+i_U}{i_L+i_U}F(\theta_I)+G(\theta_I)\right)-\frac{q_pV_G}{q_s-q_p}, \tag{6}$$

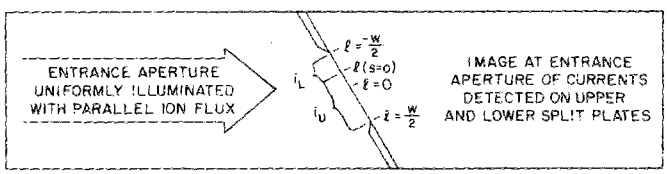

FIG. 3. Coordinate system in the detector aperture used to determine the location of the detected signal image.

$$F(\theta_I)=\frac{w(\sin\theta_a+\cos\theta_a\tan\theta_I)}{8d\sin^2\theta_I}, \tag{7}$$

$$G(\theta_I)=\frac{X_D\tan\theta_I-Y_D}{4d\sin^2\theta_I}. \tag{8}$$

Thus as described above, the plasma potential can be determined from $F(\theta_I)$ and $G(\theta_I)$, geometric factors that depend only on the entrance angle of the ions, and the measured quantities i_L, i_U, V_G, and V_A. Typical theoretical curves for these analyzer functions are shown in Fig. 4. The two local extrema shown for $G(\theta_I)$ are important characteristics in determining analyzer performance. Their locations, as functions of Y_D/X_D are shown in Fig. 5. Note that if Y_D/X_D is too large, $G(\theta_I)$ becomes a monotonically increasing function.[5] There is a range of θ_I roughly equal to twice the separation between the extrema for which the variation in $G(\theta_I)$ is small. In this angular range, the first mode of operation, where i_L is held equal to i_U, results in accurate measurements of potential without requiring precise knowledge of θ_I.

The ratio of G/F is seen in Fig. 4 to be a linearly increasing function of θ_I. It depends only on geometric factors and the tangent of θ_I:

$$G/F=-\frac{2Y_D}{w}\frac{\left[1-(X_D/Y_D)\tan\theta_I\right]}{(\tan\theta_a+\tan\theta_I)\cos\theta_a}. \tag{9}$$

Expanding $\tan\theta_I$ in a Taylor series about $\theta_I=30°$ results in an approximate expression for the analyzer of Fig. 4

$$G/F\simeq 35.63+\Delta\theta_I(1.76) \tag{10}$$

that agrees very well with the exact formula of Eq. (7) in the angular range of the plot ($\Delta\theta_I=\theta_I-30°$).

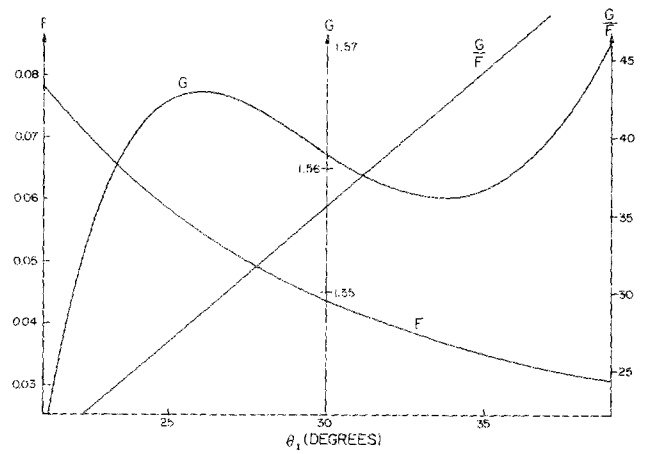

FIG. 4. Geometric functions that characterize the angular sensitivity of the analyzer [see Eqs. (7)–(9)]. The specific analyzer dimensions used for these curves are $X_D=26.286$ cm, $Y_D=4.881$ cm, $d=6.595$ cm, $w=0.500$ cm, and $\theta_I=60°$.

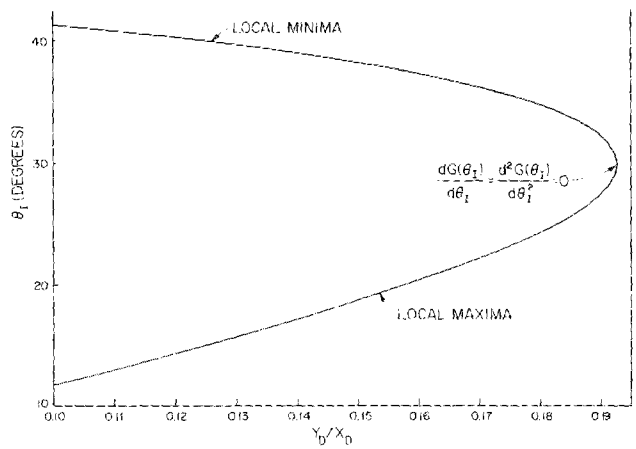

FIG. 5. Location of the extrema in $G(\theta)$ for a typical analyzer (as a function of the ratio Y_D/X_D).

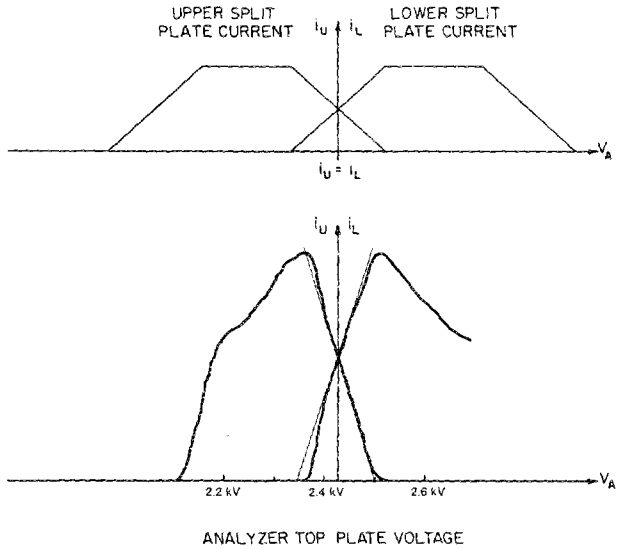

FIG. 6. Detected currents on each plate as the analyzer voltage is varied. (a) Theoretical, (b) experimental for EBT analyzer.

II. CALIBRATION

The operating characteristics of the energy analyzer can be predicted with moderate accuracy by careful manufacture and assembly of analyzer parts. However, F and G cannot be determined to the 0.01% accuracy required for application of heavy ion beam probes. It is, therefore, necessary to measure $F(\theta_I)$ and $G(\theta_I)$ in a controlled test facility and *in situ*, if possible. In most beam probe systems, the primary (charge $= +1$) ion beam can be directed into the analyzer with and without plasma. It is also necessary to incorporate adjustment of one geometric parameter in the analyzer design; X_D is easiest to vary and provides effective control of F and G.

$G(\theta_I)$ can be experimentally determined by varying V_A until $i_L = i_U$ for each realistic value of θ_I. Either active feedback or control through system software can be used for this purpose. Since the calibration experiment is performed with a charge $= +1$ ion beam, $q_s = q_p$, $\phi = 0$ and Eq. (6) simplifies to

$$\frac{i_U - i_L}{i_U + i_L} F(\theta_I) + G(\theta_I) - \frac{V_G}{V_A} = 0, \tag{11}$$

so that

$$G(\theta_I) = \left.\frac{V_G}{V_A}\right|_{i_L = i_U}. \tag{12}$$

Experimental evaluation of $F(\theta_I)$ requires a generalization of this procedure. Rather than forcing the collected currents to be equal, i_L and i_U are monitored as functions of V_A for each θ_I. Ideally, the piecewise linear plot of Fig. 6 will result. As V_A is increased, the beam formed by the entrance aperture is observed to proceed smoothly from above to below the detector plates. Note that there is a finite range of V_A for which current is collected on both plates. The value of V_A where $i_L = i_U$ can be read from this plot so that $G(\theta_I)$ can be determined. $F(\theta_I)$ is related to the slopes of $i_L(V_A)$ and $i_U(V_A)$. Taking the derivative of Eq. (11) with respect to V_A gives the necessary expression

$$F(\theta_I) = \frac{(i_L + i_U)V_G}{(di_L/dV_A - di_U/dV_A)V_A^2}. \tag{13}$$

Practical application of this expression is easiest at $i_L = i_U$ [where the slopes of $i_L(V_A)$ and $i_U(V_A)$ are equal and opposite] so both Eqs. (12) and (13) are evaluated at the same point.

A comparison of experimental $F(\theta_I)$ and $G(\theta_I)$ with theoretical predictions should be made to assure that the analyzer is operating properly. Data of the type displayed in Figs. 4 and 6 can confirm that construction and assembly have been performed successfully. It is possible to determine X_D, Y_D, d, θ_a, and w by finding the theoretical curves that best fit the data; thus even details of construction can be checked.

III. DYNAMIC RANGE AND SENSITIVITY

Measurements of plasma potential based on Eq. (6) require that ion current must be collected by both plates. This limits the range of measureable potentials to

$$\phi = \phi_{\text{center}} \pm \Delta\phi, \tag{14}$$

$$\Delta\phi \leqslant \frac{q_s V_A}{q_s - q_p} 2F(\theta_I), \tag{15}$$

$$\phi_{\text{center}} = \frac{q_s V_A G(\theta_I) - q_p V_G}{q_s - q_p}. \tag{16}$$

Thus while measurements can be made sufficiently rapidly to follow changes in ϕ that occur in times as short as 1 μs, the overall range in ϕ is limited to $\Delta\phi$. This is not a particularly severe limit since $\phi \ll V_A$, V_G and, from Eq. (16),

$$\Delta\phi \leqslant \frac{q_p}{q_s - q_p} 2 \frac{F(\theta_I)}{G(\theta_I)} V_G. \tag{17}$$

For a 100-kV primary beam and $\theta_I = 30°$, $\Delta\phi \simeq 6$ kV. An analyzer with $X_D \gg Y_D$, $\theta_a = 60°$ and operated near $\theta_I = 30°$ will have

$$\Delta\phi \leqslant (2w/X_D)V_G, \tag{18}$$

which provides a useful qualitative guide during the design process. If a very large dynamic range is required, more than

two detector plates can be used. Accurate ϕ values are then obtained as long as current is detected on at least two plates. Also some feedback or programmed control of V_A can be added to extend $\Delta\phi$.

The minimum detectable change in ϕ is determined by the ratio of signal current to noise current on the detector plates and the same factors as the maximum voltage. From Eq. (6),

$$\Delta\phi \geq \frac{q_s V_A}{q_s - q_p} 2F \frac{i_{\text{noise}}}{i_U + i_L}. \tag{19}$$

Here, i_{noise} is the minimum detectable change in $i_U - i_L$. All other terms are assumed fixed. For the same conditions as in Eqs. (16) and (17)

$$\Delta\phi \geq V_G \frac{w}{X_D} \frac{i_{\text{noise}}}{i_U + i_L}. \tag{20}$$

If the noise is plasma generated, both i_{noise} and $(i_U + i_L)$ will vary linearly with the aperture width w. In that case, making w smaller will increase sensitivity at the expense of dynamic range. If noise is only electronic in origin, then changing w will have no effect on Eq. (20) and the best possible conditions for a particular analyzer will be obtained. Note that if X_D is more than 100 times greater than w and the signal is more than 100 times the noise, sensitivity to changes smaller than 0.01% of the accelerator voltage is possible.

IV. EXPERIMENTAL RESULTS

Figure 7 shows a measured gain curve for the beam probe on EBT-S[5,6] (a toroidal confinement device at Oak Ridge National Laboratory). The accelerator and analyzer voltages were obtained using precision (0.01%) resistive dividers. Four points from the theoretical curve [Eq. (8)] that best fit the data are also shown. The curve fitting procedure is very sensitive to the choice of geometric parameters. A change in the parameter (Y_D/d) by as little as 0.04% produces a distinct error (0.1%). A properly operating analyzer can be characterized in this manner with a sensitivity of the order of a few parts in 10 000.

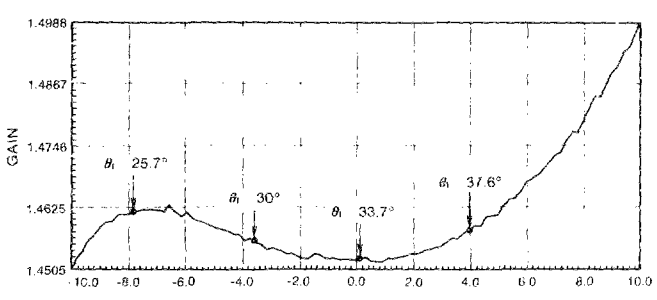

FIG. 7. Experimental gain (G) curve for EBT-S analyzer. Four theoretical points are shown for comparison [$G(30°) = 1.456$, $X_D/d = 3.711$, $Y_D/d = 0.6865$].

The data of Fig. 7 permit unequivocal identification of the unique analyzer curve and thus accurate determination of analyzer properties. This measurement must be done with great care because of the need to know the gain G with such precision. The parameter F is much smaller than G so that the application of Eq. (13) is much easier. Figure 6 also shows experimentally obtained information necessary to determine F and G for the analyzer used on EBT (an earlier version of EBT-S). There are a number of features of these data that deviate from the ideal, but none affect the measurement of F. Note first that the same slope matches both currents near the cross-over point. $F = 0.057$ while $G = 1.85$ at this entrance angle. In the central part of the data, where current is detected on both plates, the currents would have changed almost exactly linearly with analyzer voltage if the high-voltage power supply had been permitted to settle. The output is heavily filtered so that it takes a significant fraction of a second to obtain a fixed voltage. The straight sections of the data were taken very slowly. The second change from ideal is caused by the large aperture w used. There are no flat sections showing the beam walking across a single plate because the beam is the same size as the plate. Finally the asymmetries at the far left and right of the data are due partly to supply settling time and partial masking and scattering of the beam by the analyzer ground plate. The analyzer is only operated in the central section so it is not necessary to verify or even have ideal operation at other voltages.

Measurements of potential are now made almost exclusively with the new technique rather than by using a feedback controlled analyzer. In addition to the diagnostic systems on TMX[2] (a tandem mirror open confinement device at Lawrence Livermore National Laboratory) and EBT,[5,6] those on ISX[7] (a tokamak at ORNL), (Rentor)[8] (a tokamak at Rensselaer), and TEXT[9] (a tokamak at the University of Texas) have also demonstrated the increased capability of this approach.

[1] F. M. Bieniosek and K. A. Connor, Phys. Fluids **26**, 2256 (1983); R. E. Rienovsky, W. C. Jennings, and R. L. Hickok, Phys. Fluids **16**, 1772 (1973).
[2] E. B. Hooper, Jr., G. A. Hallock, and J. H. Foote, Phys. Fluids **26**, 314 (1983).
[3] T. S. Green and G. A. Proca, Rev. Sci. Instrum. **41**, 1409 (1970).
[4] F. C. Jobes and R. L. Hickok, Nucl. Fusion **10**, 195 (1970).
[5] F. M. Bieniosek, P. L. Colestock, K. A Connor, R. L. Hickok, S. P. Kuo, and R. A. Dandl, Rev. Sci. Instrum. **51**, 206 (1980).
[6] J. R. Goyer, Ph.D. thesis, Rensselaer Polytechnic Institute, 1984.
[7] G. A. Hallock, J. Mathew, W. C. Jennings, R. L. Hickok, A. J. Wootten, and R. C. Isler, Phys. Rev. Lett. **56**, 206 (1986).
[8] J. D. Michael, E. Saravia, R. L. Hickok, and W. C. Jennings, Rev. Sci. Instrum. **57**, 1828 (1986).
[9] P. M. Schoch, J. C. Forster, W. C. Jennings, and R. L. Hickok, Rev. Sci. Instrum. **57**, 1825 (1986).